Effect of Wall Roughness on the Dynamics of Unsteady Cavitation

Olivier Coutier-Delghosa, Jean-François Devillers, Mireille Leriche, Thierry Pichon

Effect of Wall Roughness on the Dynamics of Unsteady Cavitation

Olivier Coutier-Delgosha, Jean-François Devillers, Mireille Leriche, Thierry Pichon

ENSTA - UER de Mécanique Chemin
de la Hunière,
91761 Palaiseau Cedex, France

The present paper is devoted to the experimental study of unsteady cavitation on the suction side of a two-dimensional foil section positioned in a cavitation tunnel with a small incidence angle. When the pressure is decreased in the tunnel, a sheet of cavitation characterized by large amplitude fluctuations is obtained on the foil. The present study focuses on the effects of the foil wall roughness on the cavity unsteady behavior. Four different sizes d of irregularities have been tested, from the smooth surface to a 400 μm *grain size. The characteristic frequency of the flow unsteadiness is investigated by ana-lyzing the data measured by a pressure transducer mounted flush on one vertical wall of the test section, whereas the mean cavity length is obtained by visual measurements on the foil side. Several types of cloud cavitation are identified in the case of the smooth surface. The effect of roughness is a significant decrease of the cavity length and a large increase of the oscillation frequency. It results in Strouhal numbers higher than the classical values obtained for partial cavity fluctuations. Moreover, the cavitation cycle is disorganized by the increase of the roughness, as it can be detected by the fast fourier transform analysis of the pressure signal. The general effect is a reduction of the pressure fluctuation intensity.*

1 Introduction

Rocket-engine turbopumps are generally equipped with an inducer stage that operates in cavitating conditions because of the low pressure of the fluid at the inlet of the pumps. Cavitation mainly consists in vaporized areas on the suction side of the blades, usually denoted sheets of cavitation (Fig. 1). Additional low-pressure areas, such as the tips of the blades and the gap between the rotor and the stator, also exhibit cavitation. Two major types of instability due to cavitation have been detected in inducers. The first one consists in nonsymmetrical flow arrangements (one little sheet of cavitation and three large ones, for example, in the case of a four-blade inducer) that rotate with a speed different from that of the pump, as explained, for example, by de Bernardi et al. [1]. The second one is based on large amplitude fluctuations of the sheets of cavitations on the blades, which result in significant pressure fluctuations at the outlet of the inducer. These fluctuations may deteriorate the operation of the other stages of the turbopump, so they must be avoided or at least controlled.

The second category of instability has been extensively investigated in cavitation tunnels by analyzing the flow around two-dimensional foil sections [2–5] or Venturi-type sections [6–9]. In both configurations, the sheet cavity on the foil suction side or the Venturi throat is characterized by cyclic oscillations, whose frequency mainly depends on the cavity length. According to these previous studies, the periodic fluctuations of the cavity are driven by a reentrant jet that regularly flows from its downstream end up to the foil leading edge, close to the wall. This reverse flow thus periodically cuts the cavity interface in its upstream part, which results in the detachment of the rear part. The resulting cloud of vapor is then convected downstream until it encounters an adverse pressure gradient and collapses. Other mechanisms, such as the destabilization of the cavity interface combined with the reentrant jet, have also been proposed by Lush and Peters [7] to explain the self-sustained oscillations. The role of shock waves due to the collapse of the cloud of vapor is also investigated by Song and Qin [10] on the basis of numerical simulations.

To control the self-oscillating behavior by stopping the reentrant jet is the basic idea that was proposed by Kawanami et al. [2]. These authors experimented with the use of obstacles characterized by a significant height (2 mm) to prevent cloud cavitation. The objective was reached even with a little length of the obstacle in the spanwise direction, which confirms that the flow unsteadiness is mainly triggered by the reentrant jet. Similar results were obtained by Pham et al. [3] with the same type of obstacle: a modification of the cloud-shedding phenomenon was observed, associated with a large reduction of the reverse flow momentum. Recently, Stutz [11] analyzed the effects of using striated or rough bottoms instead of a polished one in a Venturi-type section. No noticeable influence of these parameters on the two-phase flow structure was detected. However, the irregularities on the surface were, in this case, much smaller than the characteristic size of the obstacle used by Kawanami et al. [2].

The present paper focuses on the experimental investigation of the effects of the roughness of the foil surface on the dynamics of the cavitating flow. Experiments are conducted in the ENSTA cavitation tunnel where various cavitation conditions can be obtained: pressure can be lowered down to 150 mbar and the flow velocity can be increased up to 10 m/s. Although the shape of the foil section is very simple (Fig. 2), its sharp leading and trailing edges and small angle of attack make it representative for the flow over the blades of a rocket-engine turbopump inducer. This is the main advantage of using a foil section, instead of a Venturi-type section.

When the pressure is decreased in the cavitation tunnel, sheet cavitation appears on the foil suction side. Its behavior is rather steady at small incidence, with only small-scale fluctuations in its rear part, whereas periodical self-oscillations of large amplitude involving vapor cloud shedding are obtained when the angle of attack is increased. Figure 3 presents side views of the flow corresponding to the successive steps of the cycle for an angle of attack α=3 deg, an inlet velocity V_{ref}=6 m/s and a cavitation number σ=1. The limit between stable and unstable configurations is usually contained in the range 2–3 deg. The foil suction side is equipped with interchangeable plates characterized by different roughness. This device enables one to investigate the effect

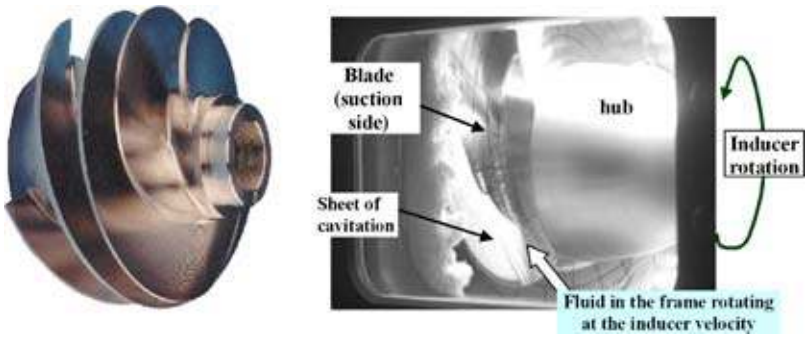

Fig. 1 (*a*) Geometry of a rocket-engine turbopump inducer, (*b*) cavitating flow

of the roughness on the cavity dynamics in order to determine whether irregularities of the surface modify the progression of the reentrant jet or not.

Section 2 is devoted to the presentation of the experimental setup and estimation of the measurement uncertainties. Results obtained with the smooth surface are presented in Sec. 3, and Sec. 4 focuses on the effects of roughness.

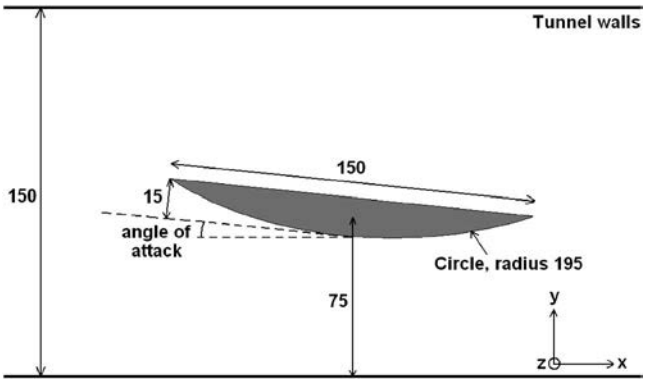

Fig. 2 Foil geometry

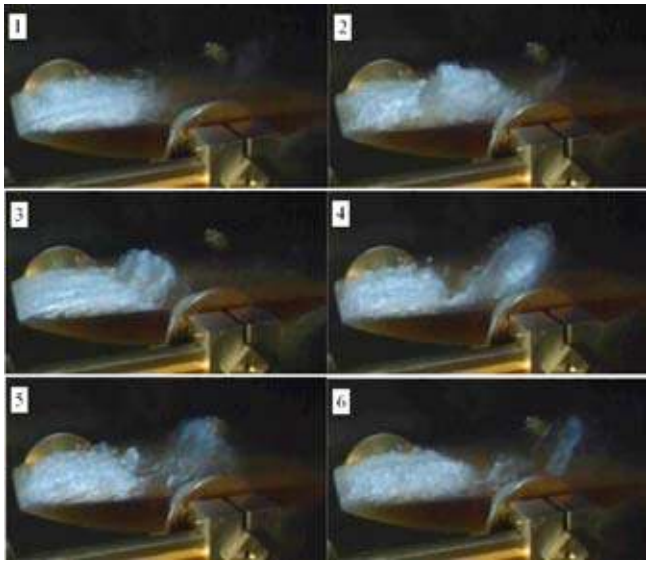

Fig. 3 Vapor cloud shedding on the foil suction side (Incidence 3 deg, V_{ref}=6 m/s, σ=1)

2 Experimental Setup

The considered geometry is a two-dimensional foil of 150 mm chord and 80 mm span. Its cross section is composed of a flat upper surface and a convex lower surface of 195 mm radius, as illustrated by Fig. 2. Experiments were performed in the ENSTA cavitation tunnel whose test section is 150 mm height, 80 mm width, and 640 mm length. The foil was located at midheight, with a small angle of attack, so a cavitation sheet appears on the upper face, when the pressure is decreased in the tunnel. Compared to the Venturi configuration, studied previously by Stutz and Reboud [8,9], the cavitation behavior is modified by the possible interaction between the foil pressure and suction sides.

The upper wall of the foil section is equipped with interchangeable plates characterized by various roughnesses. Preliminary tests have been performed with abrasive paper sized on the foil, but cavitation systematically resulted in its destruction. In the present case about 55% of the foil surface is covered by the plates, which are screwed, as indicated in Fig. 4. Four plates with various

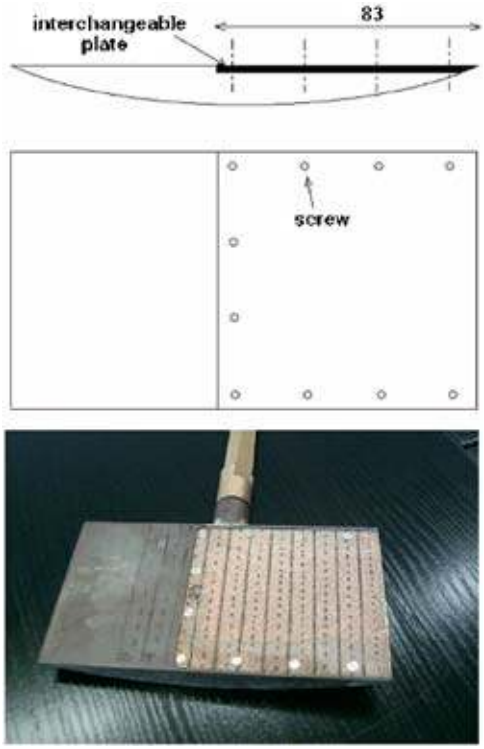

Fig. 4 (*a*) Scheme of the adaptable foil section, and (*b*) view of the foil

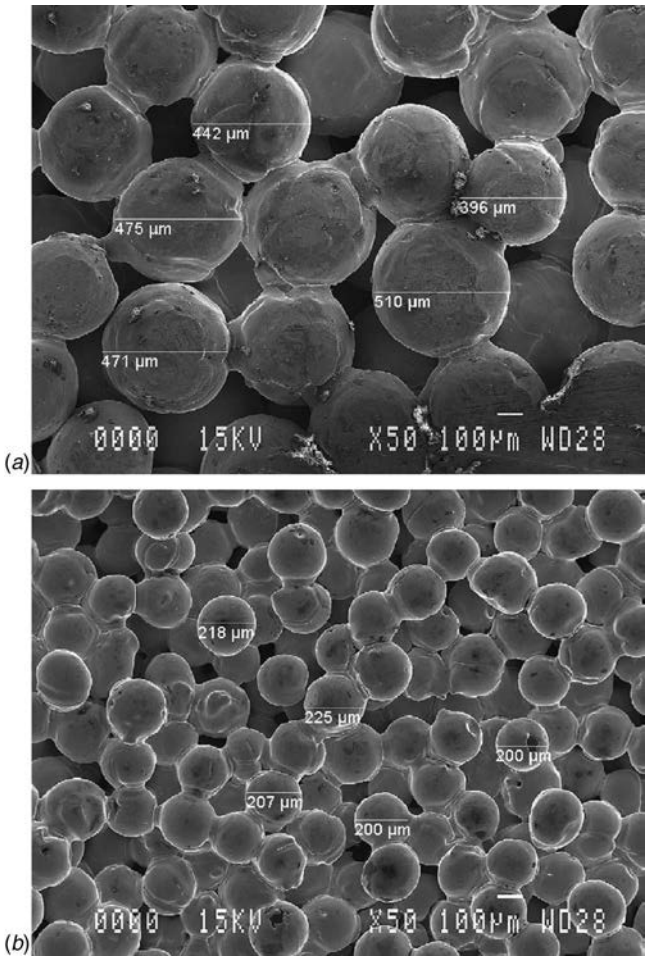

Fig. 5 Detail of the roasted metal (microscope, magnitude 50) (*a*) Mean grain size 400 μm, and (*b*) mean grain size 200 μm

roughnesses and a fifth one, perfectly smooth, are available. Roughness is obtained by metal roasting based on the compression of microscopic brass balls close to the melting conditions. Roughness can thus be defined in the present experiments by the mean diameter d of the balls, like the grain size in the Nikuradse's sand roughness [12]. The detail of the protrusions, obtained by a microscope with magnitude $\times 50$, can be seen in Fig. 5. Four ball diameters are considered, namely, $d=100$, 200, 300, and 400 μm. They are denoted hereafter "Roughness 100, 200, 300, 400." These values result from a preliminary study based on the work of Schlichting, who indicates a condition to obtain a completely rough regime characterized by protrusions larger than the laminar viscous sublayer. This condition is given by a minimum Reynolds number $\mathrm{Re}=V_{\mathrm{ref}}\times d/\nu=100$, where ν denotes the kinematic viscosity of the fluid. In the experiments $V_{\mathrm{ref}}=6$ m/s and $\nu=10^{-6}$ m^2/s so the minimal size of the balls should be ~ 16 μm.

Another foil composed of a single piece with a smooth upper face is also used to check that the fixation of the plates has a negligible influence on the behavior of the cavity. The reference pressure P_{ref} is measured with a JPB model TB 142 absolute pressure sensor connected to two pressure taps located, respectively, at the bottom and at the top of the test section inlet. These two taps enable one to take into account the effect of a possible velocity gradient in the height of the cavitation tunnel. The reference velocity V_{ref} is derived from the mass flow rate Q and the size of the cross section of the test section inlet. Q is controlled by a propeller flow meter. These flow conditions are regulated with 3% and 1% precision respectively, for P_{ref} and V_{ref}, which leads to a 5% uncertainty on the cavitation number $\sigma=(P_{\mathrm{ref}}-P_{\mathrm{vap}})/(\frac{1}{2}\rho V_{\mathrm{ref}}^2)$, where P_{vap} denotes the vapor pressure and ρ the water density.

The unsteady behavior of cavitation is characterized by measurements of the fluctuating pressure with a PCB model M106B50 piezoelectric pressure transducer whose resonant frequency is 40 kHz and sensibility is 0.07 mV/Pa. The transducer is mounted flush on one of the vertical walls of the test section, 30 mm upstream the foil leading edge. The pressure data are processed by a HP 35665 spectrum analyzer whose frequency full span and default resolution are, respectively, 102.4 kHz and 400 lines. No filtering is applied to the pressure signal. To obtain the frequency f of the cavity self-oscillation, Fourier transforms are performed from 1024 sample data and then averaged over 40 tests.

The length L_{cav} of the sheets of cavitation is estimated visually using signs painted on the foil surface each 5 mm. In this work, L_{cav} denotes the maximum length of the leading edge cavity, i.e., the part that remains attached to the foil, without considering the wake downstream. To estimate the uncertainty concerning this measurement, another method is applied in the case of the smooth foil surface. For each flow condition, 60 side views and top views of the sheet cavity are recorded with a standard B&W CCD camera operating at 25 fps. The mean shape and thus the mean length L_{cav} of the vaporized area are obtained by averaging the gray levels on these 60 random pictures and then applying a filter to the resulting picture (see Fig. 6). The results obtained by the three methods are compared in Fig. 7 in the configuration $\alpha=6$ deg for σ varying between 1.6 and 1. A reliable agreement is obtained for small cavities, whereas the uncertainty is significantly increased for large sheet cavities, mainly because of their large amplitude fluctuations. On the basis of this result, the precision of the direct measurements is finally estimated to be 8%.

The setup presented here was exploited during two sets of measurements achieved with different experimental procedures:

- For set 1, the flow was investigated by successively using the smooth foil, and three plates with, respectively, a smooth surface, $d=200$ μm, and $d=400$ μm. A large range of cavitation numbers was tested, from $\sigma=1.8$ down to $\sigma=0.7$. The angle of attack was varied between 0 and 6 deg by steps of 1 deg, and the reference velocity V_{ref} was equal to 6 m/s.
- For set 2, the cavitation number was $\sigma=1.3$ and $V_{\mathrm{ref}}=6$ m/s. Four plates have been tested (the smooth one, and $d=100$, 200, and 400 μm) with an angle of attack ranging from $\alpha=0$ to 5 deg by steps of 0.25 deg.

3 Results With the Smooth Wall

In this section, the results obtained in the case of the smooth foil section (without the setup for the interchangeable plates) are presented. They were obtained in conditions similar to the ones reported previously by Pham et al. [3]. However, the present experiments indicate that the unsteady behavior of the cavitation sheet is characterized by three different types of oscillations, which depend both on the cavity length and the cavitation number σ.

Six values of the cavitation number are investigated from $\sigma=1.8$ down to $\sigma=0.7$. The reference velocity V_{ref} is kept equal to 6 m/s. For each flow condition, the angle of attack is varied from $\alpha=0$ deg up to $\alpha=0$ deg by steps of 1 deg (measurement set 1). Sheet cavitation on the foil suction side appears for a very low incidence usually close to 1 deg. No significant unsteadiness can be detected on the pressure signal for angles lower than 2 deg: only high-frequency perturbations (between 200 and 500 Hz) are obtained. This is because of small-scale fluctuations in the rear part of the cavity, as previously reported by De Lange et al. [13] and Pham et al. [3]. When the angle of incidence is increased over 2 deg, large fluctuations of the cavity length are observed, while

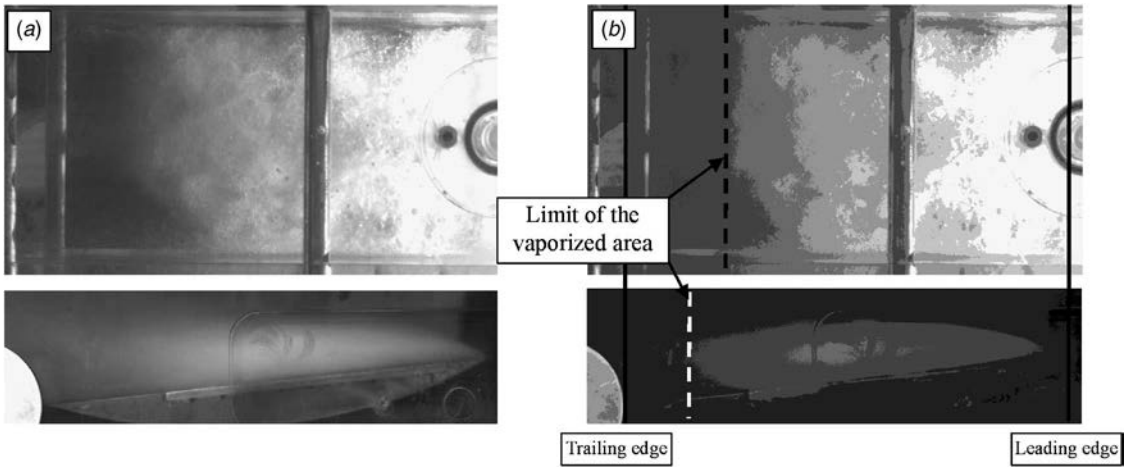

Fig. 6 Estimation of the cavity length from top and side views of the cavity (α=6 deg, σ=1) (*a*) initial pictures, (*b*) postprocessing to visualize the limit of the cavity

the spectra of the fluctuating pressure signal exhibit one or several sharp dominant peaks. The corresponding frequencies decrease when the cavity length is increased, i.e., when the angle of attack is augmented. This behavior is systematically obtained for all cavitation numbers.

We focus hereafter on the conditions that lead to a pronounced flow unsteadiness characterized by large-scale fluctuations involving periodical vapor cloud shedding (2 deg $< \alpha <$ 6 deg). Such behavior is usually referred to as cloud cavitation in previous studies [3,8,9]. Figure 8 presents the evolution of the cavity length according to the cavitation number σ and the incidence α. The values are plotted as a function of the parameter σ/α, derived from the one ($\sigma/2\alpha$) proposed by Acosta [14] in his linearized theory of partial cavitation on flat-plate hydrofoils. Le et al. [15] have more recently correlated the cavity length L_{cav} with the parameter σ/α, in the case of hydrofoils similar to the present one. This result is confirmed by the present experiments, since the cavity lengths measured in all flow conditions are very close to a unique chart, which suggests that they only depend on σ/α. The data scattering may be mainly due to the 8% measurement uncertainty on L_{cav}. Note also that the foil angle of attack is known with a 1% precision and σ with a 5% precision (see Sec. 2), so the uncertainty on σ/α is about 6%. The chart represented by the solid line is a polynomial approximation of the experimental points, and its equation is

$$\frac{L_{cav}}{L_{ref}} = \frac{A}{\left(\frac{\sigma}{\alpha}\right)^n} \tag{1}$$

with $A \approx 100$ and $n \approx 2$.

The dynamics of the sheet of cavitation is investigated in Fig. 9 by plotting the Strouhal number $\mathrm{Str} = f \times L_{cav}/V_{ref}$ as a function of σ/α. The frequency f is the one corresponding to the dominant peak on the spectrum of the pressure signal. Actually, several peaks are often obtained with different magnitudes. In such cases only the dominant peak with the highest amplitude is considered. The only exception concerns the very large cavities ($L_{cav}/L_{ref} > 75\%$), since in these cases the spectra suddenly exhibit a supplementary peak of much higher amplitude than all others. This is due to a new type of instability in the flow; therefore, in these configurations this peak and the dominant one of lower amplitude are both regarded.

Several different behaviors can be distinguished:

i. For σ lower than 1.3, a single sharp dominant peak of large magnitude is usually obtained, leading to a Strouhal number very close to a value of 0.25, which is the most classical one for cloud cavitation [3,8]. The Strouhal num-

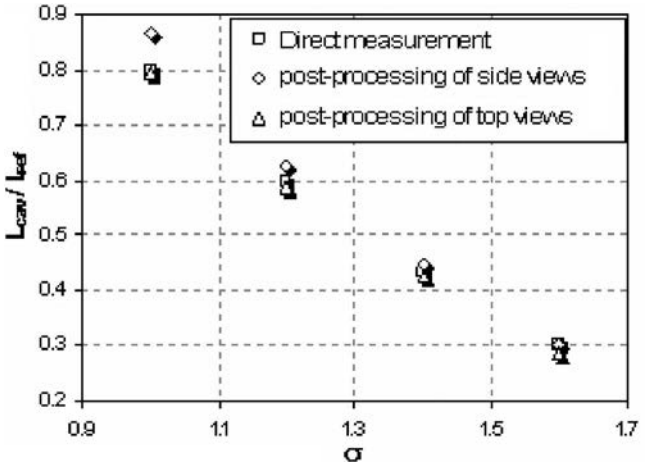

Fig. 7 Comparison of the cavity lengths obtained (i) by direct measurements, (ii) by postprocessing of side and top views of the cavity

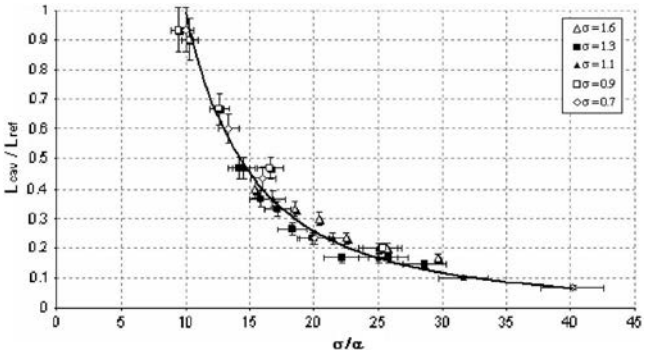

Fig. 8 Evolution of the maximum attached cavity length for several flow conditions and angles of attack varying from 2–6 deg (measurement set 1)

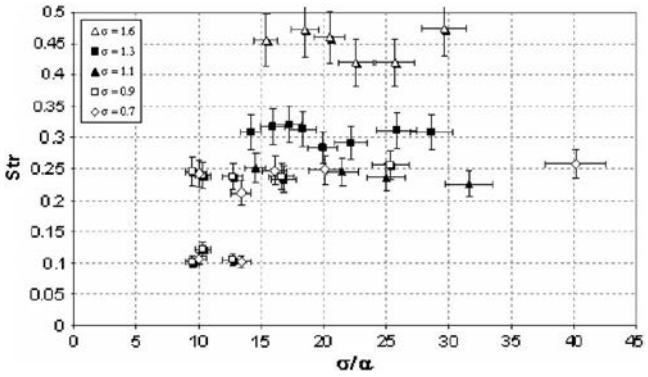

Fig. 9 Strouhal number associated with the cavity self-oscillation (measurement set 1)

ber is almost constant in this configuration, and no influence of the cavitation number σ is detected.

ii. For σ higher than 1.3 (only $\sigma=1.3$ and $\sigma=1.6$ are represented here), the Strouhal number progressively increases, while the magnitude of the dominant peak decreases significantly and the number of secondary peaks of comparable amplitude increases. Visually, in this situation the flow remains clearly unsteady, whereas the large-scale fluctuations seem to be weaker. However, the value of the Strouhal number is still almost constant for a given value of σ ($St\approx 0.3$ for $\sigma=1.3$ and $St\approx 0.45$ for $\sigma=1.6$). The diminution of the dominant peak magnitude suggests that only a part of the cavity is affected by the vapor shedding. This would explain the acceleration of the cavitation cycle. Strouhal numbers based on the size of the unstable rear part of the cavity instead of its maximum length may result in recovering the value $St=0.25$.

iii. In the case of very large sheets of cavitation (mainly at low cavitation number $\sigma\leqslant 0.9$ and high angle of attack $\alpha\geqslant 4$ deg), a new dominant peak of great intensity is obtained in the spectra, while the standard peak corresponding to $St=0.25$ is still present. This new peak is associated with a lower frequency that leads to a Strouhal number close to 0.10/0.12. It characterizes a trailing-edge instability due to the interaction between the foil suction and pressure sides. It has been shown recently by numerical simulations [16] that such an interaction governs the whole cavitation cycle by periodically imposing a low-pressure level at the foil trailing edge. As a result, the adverse pressure gradient in the rear part of the cavitation sheet is too weak to enable the progression of the reentrant jet under the cavity toward the leading edge. This progression, which is responsible for the cavity break-off, is only possible when the trailing-edge interaction periodically decreases. So the entire cavitation cycle adopts the frequency of the trailing-edge instability. This phenomenon is usually intermittent when the cavity length is about 80%, which explains that two peaks corresponding, respectively, to $St\approx 0.25$ and $St\approx 0.11$ appear on the spectra, whereas it is almost permanent when the cavity length is still increased.

The low Strouhal number reported in iii is similar to the normalized frequency $f\times L_{ref}/V_{ref}\approx 0.1$ obtained theoretically by Watanabe et al. [17] in the case of very large sheets of cavitation. Actually, these authors distinguish the "partial cavity oscillations," corresponding to cloud cavitation with $L_{cav}/L_{ref}<75\%$, from "transitional cavity oscillations," occurring for sheets of cavitation larger than 75% of the chord and characterized by a lower Strouhal number. These expressions will be used hereafter in the present work to differentiate the two behaviors.

4 Effects of Roughness

Both measurement sets 1 and 2 are analyzed in this section in order to investigate the effect of the surface roughness on the cavity dynamics. The first step consists of checking the influence of the irregularities due to the fixation of the plate on the foil. So the smooth plate is first used, and the characteristics of the sheet cavitation are compared to the results presented in the previous section. Figure 10 shows the evolution of the cavity length according to the parameter σ/α for three values of σ (0.9, 1.1, and 1.3). The polynomial approximation obtained in the case of the other foil is also reported in dashed line. All these results belong to the measurement set 1. No significant discrepancy is observed, apart from a slight general increase of the lengths, which is systematically smaller than the uncertainty on their measurement.

It is then checked in Fig. 11 that the surface roughness does not induce any supplementary effect of the cavitation number on the cavity length: its evolution is drawn according to σ/α in the case $d=400$ μm. Results corresponding to $\sigma=0.9$, 1.1, and 1.3 are reported. All the points almost form a single curve whose approximation is indicated in solid line, so the cavity length depends only on σ/α, as in the previous case of the smooth surface.

Figure 12 presents the evolution of the cavity length as a function of the angle of attack α, with four different plates. Although

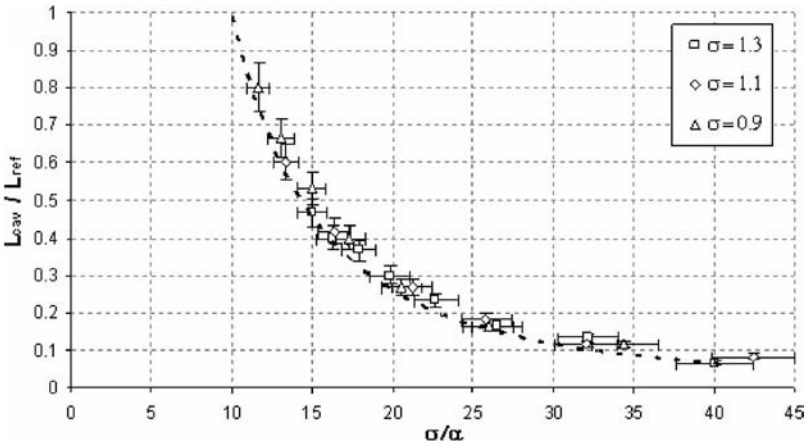

Fig. 10 Evolution of the maximum attached cavity length on the foil equipped with the smooth plate (measurement set 1). The dashed line corresponds to the approximation curve plotted previously on Fig. 8.

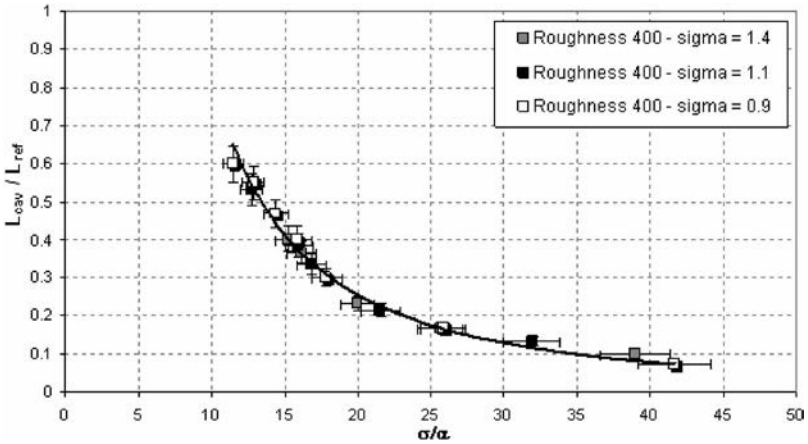

Fig. 11 Cavity lengths for roughness 400 and three values of σ (measurement set 1)

the present results focus on a single value of $\sigma=0.8$ (measurement set 2), similar conclusions have been obtained for higher values of σ. It can be observed that the size of the cavity only slightly depends on the roughness when $\alpha<2.5$ deg, i.e., when only small-scale fluctuations affect the sheet of cavitation. However, as soon as large amplitude oscillations start, significant discrepancies are obtained: L_{cav} is much lower with roughness 200 and 400 than with the smooth plate. The difference is about 40–50 % for 2.5 deg $<\alpha<4$ deg. This gap is partially reduced for $\alpha>4$ deg, and it equals only 25% for $\alpha=5$ deg. The case of roughness 100 gives intermediate values of L_{cav}. Two conclusions can be derived from this evolution: (i) roughness affects significantly the cavity length only in conditions of cloud cavitation and (ii) the effect of roughness does not linearly depend on the size of the protrusions; a noticeable modification of the cavity length is obtained by increasing d from 0 to 200 μm, but it seems that increasing d over 200 μm does not lead to any substantial evolution.

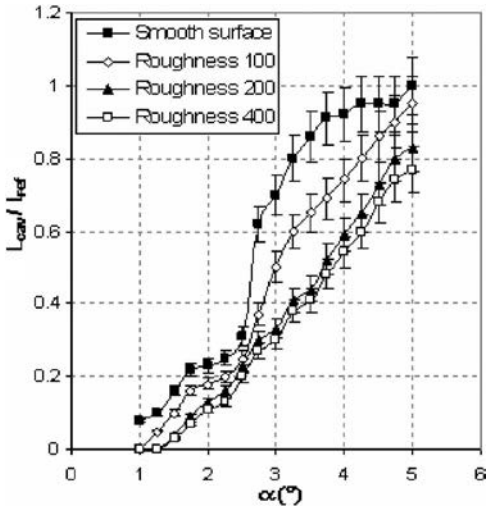

Fig. 12 Evolution of the cavity length with the incidence for $\sigma=0.8$ and three different plates of various roughnesses (measurement set #2)

When the sheet cavitation becomes longer than the plates, the cavity continues to increase in the case of roughness 400, whereas it almost stabilizes on the smooth plate. However, the discrepancy between roughness 400 and 100 remains approximately constant. Thus, these results do not indicate clearly if the end of the roughness at 55% of the foil plays a major role or not.

The analysis of the Strouhal numbers obtained for $\sigma=0.9$ and 1.3 (Figs. 13 and 14, respectively) shows a major effect of roughness on the cavity dynamic. Note that the first flow condition was characterized previously by a constant Strouhal number St ≈ 0.25, whereas the second one, and higher values of σ, resulted in a progressive increase from St ≈ 0.25 up to St ≈ 0.45 for $\sigma=1.6$. Both roughnesses 200 and 400 clearly lead here to a notable augmentation of these values: St is about 0.35–0.45 for $\sigma=0.9$,

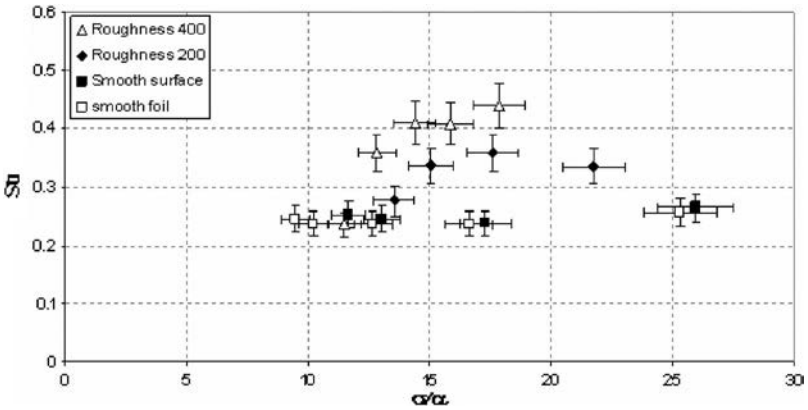

Fig. 13 Strouhal numbers for various roughness and $\sigma=0.9$ (measurement set 1)

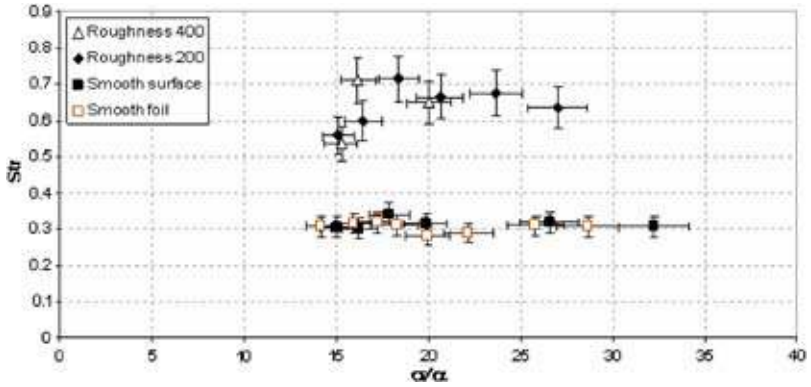

Fig. 14 Strouhal numbers for various roughness and $\sigma=1.3$ (measurement set 1)

and 0.55–0.75 for $\sigma=1.3$. Although the data are scattered into these ranges, this discrepancy with the previous results cannot be attributed to the experimental uncertainties (see Figs. 13 and 14). It indicates that the protrusions make the shedding frequency much increase. This result must be associated with the visual observations, which display a notable modification of the aspect of the cavity. Its downstream end is not so clearly limited as before, and the noise resulting from the self-oscillations seems to be significantly weaker. This trend is confirmed by the spectra of the fluctuating pressure signal; the sharp dominant peaks have been replaced by dominant frequencies distributed in broad ranges of a few tens of hertz width and characterized by much lower magnitudes (see Fig. 15). As a matter of fact, these magnitudes are divided by a factor comprised between three and five when d is increased from 0 to 400 μm. This modification, which can be interpreted as a reduction of both intensity and regularity of the cavitation cycle, suggests that the shedding process is strongly perturbed by roughness. This may be due to a premature decrease of the reentrant jet momentum because of the additional stress induced by the protrusions. As a result, only a small part of the cavity is detached from the foil. Such small vapor shedding (close to the one observed at low incidence) is usually characterized by a high and fluctuating frequency, which explains both the high Strouhal numbers and the modification of the pressure signal spectra. The general effect that may be interesting for spatial applications is a large reduction of the pressure fluctuations in the tunnel.

Figure 16 presents for $\sigma=0.8$, the Strouhal number evolution according to the angle of attack. Three values of roughness and the smooth plate are considered (measurement set 2). This figure confirms that St strongly increases when roughness is augmented. However, this effect is only present for $\alpha>2.5$ deg (beginning of the unsteadiness) and $\alpha<4$ deg (cavity smaller than the plates). For a higher incidence, a constant value close to 0.25–0.3 is recovered in all cases. It indicates that the surface roughness in the downstream end of the cavity is the dominant parameter that governs the modification of the cavitation cycle. For a sheet cavity longer than 60% of the chord, the smooth surface in the rear part enables a correct initial progression of the reverse jet and then no modification of the oscillations is obtained. It suggests that the reentrant jet is affected by roughness only in the cavity closure area. This may be due to an increase of its thickness during its progression toward the leading edge, which makes it less sensitive to the friction caused by the protrusions. The configuration of transitional cavity oscillations with roughness, which is not reported in Fig. 16, also leads to nonmodified Strouhal numbers close to 0.11. This is not surprising, since such cavities are much longer than the rough plates.

Other information given by Fig. 16 concerns the inception of cloud cavitation. The angle of attack α at which it occurs progressively increases when roughness is augmented (1.75 deg for the

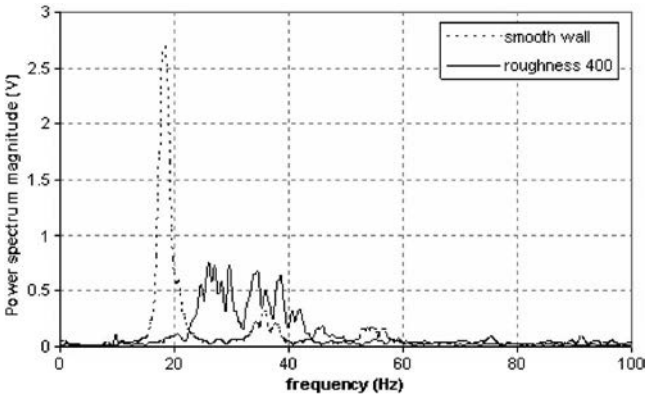

Fig. 15 Spectra of pressure signal fluctuations at incidence 5 deg and $\sigma=1$ with (*a*) a smooth surface ($L_{cav}/L_{ref}=0.7$) and (b) roughness 400 ($L_{cav}/L_{ref}=0.55$)

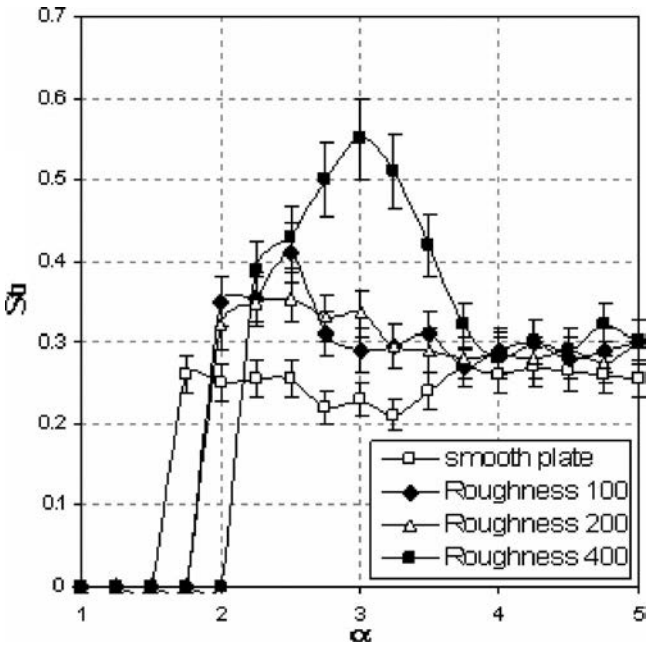

Fig. 16 Strouhal numbers for various roughness and $\sigma=0.8$ (measurement set 2)

smooth plate, 2.25 deg for roughness 400). Below this limit, only high-frequency fluctuations with no dominant peak on the spectra are obtained. This is a supplementary indication of the destabilization of the cavitation cycle in the case of a rough wall: periodical oscillations require a minimum angle of attack slightly higher than in the case of the smooth wall. This is consistent with the diminution of the reentrant jet momentum due to friction discussed previously.

5 Conclusion

The effect of the surface roughness on the dynamics of sheet cavitation on a two-dimensional foil section was investigated in this paper. We have focused mainly on cloud cavitation conditions, characterized by large amplitude oscillations involving periodical vapor cloud shedding. Acquisitions are based on cavity-length measurements and analysis of the spectra given by the fluctuating pressure signal in the cavitation tunnel. A careful analysis of several sets of measurements was performed in order to identify (i) the different unsteady behaviors in the case of a smooth foil and (ii) the modification of these behaviors due to roughness.

Concerning the first point, it has been found that cavitation numbers σ lower than 1.3 systematically lead to Strouhal numbers close to 0.25; thus far, the sheet of cavitation remains smaller than about 80% of the chord. In the case of larger cavities, a new frequency due to the interaction between the foil pressure and suction sides is obtained, which gives Strouhal numbers ranging from 0.1 to 0.12. The first configuration corresponds to partial cavity oscillations, while the second one is similar to transitional cavity oscillations, according to the theoretical work of Watanabe et al. [17]. Cavitation numbers higher than 1.3 lead to a progressive increase of the Strouhal numbers. In all cases the cavity length only depends on the parameter σ/α.

Concerning the second point, it has been noticed that roughness induces a significant diminution of the cavity length, associated with a clear increase of the Strouhal numbers. This second effect has been observed mainly for a self-oscillating cavity whose length is smaller than the one of the rough plates, which indicates that roughness in the downstream end of the sheet cavity plays a major role in the arrangement of the cavitation cycle. The general effect of roughness is a disorganization of the periodical shedding, characterized by much lower pressure fluctuations than previously. It has been suggested that the protrusions, which are here much larger than the viscous sublayer width, cause an increase of the friction experienced by the reentrant jet. The premature decrease of the reentrant jet momentum would thus be responsible for the modification of the cavity dynamics.

Acknowledgeents

This work was performed with the contribution of successive teams of students from ENSTA (Ecole Nationale Supérieure de Techniques Avancées) and l'Ecole Navale (French Naval academic school). They are all associated with this study. The measurement set 1 corresponds to the data obtained by T. Federici and R. Meireles [18] during their second year research project, while the measurement set 2 was obtained by L. Bouchentouf [19] during his Master's project.

Nomenclature

d = mean size of the protrusions on the rough plates, m
f = frequency of the cavity oscillations, Hz
$L\text{ref}$ = chord length of the foil, m
L_{cay} = maximum length of the attached cavity, m
P_{ref} = reference pressure at the inlet of the test section, Pa
P_{vap} = vapor pressure, Pa
Q = mass flow rate in the tunnel, m^3/s
Re = Reynolds number $L_{\text{ref}} \times V_{\text{ref}}/v$
St = Strouhal number $f \times L_{\text{cav}}/V\text{ref}$
V_{ref} = reference velocity based on the mass flow rate, m s^{-1}
α = foil angle of attack
v = kinematic viscosity, m^2/s
ρ = density, kg m^{-3}
σ = cavitation number

References

[1] de Bernardi, J., Joussellin, F., and Von Kaenel, A., 1993, "Experimental Analysis of Instabilities Related to Cavitation in Turbopump Inducer", *Proc. of 1st Int. Symp. on Pump Noise and Vibrations, Paris, France*, pp. 91–99.

[2] Kawanami Y., Kato H., Yamaguchi H., Tayaga Y., and Tanimura M., 1997, "Mechanism and Control of Cloud Cavitation," ASME J. Fluids Eng., **119**, pp. 788–794.

[3] Pham, T. M., Larrarte, F., and Fruman, D. H., 1999, "Investigation of Unstable Sheet Cavitation and Cloud Cavitation Mechanisms," ASME J. Fluids Eng., **121**, pp. 289–296.

[4] Laberteaux, K. R., and Ceccio, S. L., 2001, "Partial Cavity Flows, Part 1. Cavities Forming on Models Without Spanwise Variation," J. Fluid Mech. vol **431**, pp. 1–41.

[5] Leroux, J-B., Astolfi, J-A., and Billard, Y., 2004, "An Experimental Study of Unsteady Partial Cavitation," ASME J. Fluids Eng. **126**, 94–101.

[6] Furness, R. A., and Hutton, S. P., 1975, "Experimental and Theoretical Studies of Two-Dimensional Fixed-Type Cavities," ASME J. Fluids Eng. **97**, pp. 515–522.

[7] Lush, P. A., and Peters, P. I., 1982, "Visualization of the Cavitating Flow in a Venturi Type Duct Using High-Speed Cine Photography", *Proc. of International Association of Hydraulic Engineering and Research Conference on Operating Problems of Pump Stations and Power Plants*, Amsterdam, Netherlands, **5**, pp. 1–13.

[8] Stutz, B., and Reboud, J-L., 1997, "Experiments on Unsteady Cavitation," Exp. Fluids **22**, pp. 191–198.

[9] Stutz, B., and Rebound, J-L., 2000, "Measurements Within Unsteady Cavitation," Exp. Fluids, **29**, pp. 545–552.

[10] Song, C. C. S., and Qin, Q., 2001, "Numerical Simulation of Unsteady Cavitating Flow," *Proc. of 4th Int. Symp. on Cavitation*, California Institute of Technology, Pasadena, http://cav2001.library.caltech.edu/

[11] Stutz, B., 2003, "Influence of Roughness on the Two Phase Flow Structure of Sheet Cavitation," ASME J. Fluids Eng., **125**, pp. 652–659.

[12] Schlichting, H., 1979, *Boundary layer theory*, McGraw-Hill Series in Mechanical Engineering, Seventh Edition.

[13] De Lange, D. F., Bruin, G. J., and Van Winjngaarden, L., 1994, "On the Mechanism of Cloud Cavitation-Experiment and Modeling," *Proc. of 2 Int. Symp. on Cavitation*, Tokyo, Japan, H. Kato, ed., pp. 45–49.

[14] Acosta, A., J., 1955, "A Note on Partial Cavitation of Flat Plate Hydrofolis," California Institute of Technology, Report N° E-19.9.

[15] Le, Q., Franc, J. P., and Michel, J. M., 1993, "Partial Cavities: Pressure Pulse Distribution Around Cavity", ASME J. Fluids Eng. **115**, pp. 249–254.

[16] Coutier-Delgosha, O., Devillers, J-F., Pichon, T., Vabre, A., Woo, R. and Legoupil, S., "Internal Structure and Dynamics of Sheet Cavitation," Phys. Fluids (submitted).

[17] Watanabe, S., Tsujimoto, Y., and Furukawa, A., 2001, "Theoretical Analysis of Transitional and Partial Cavity Instabilities," ASME J. Fluids Eng. **123**, pp. 692–697.

[18] Federici, T., and Meireles, R., 2003, "Cavitation sur profil portant," unpublished.

[19] Bouchentouf, L., 2003, "Influence de la rugosité sur le développement des poches de cavitation sur les hydrofoils," Master report, Ecole centrale de Nantes.